Geoid
Journal of Geodesy and Geomatics

Geoid Vol. 20, No. 2, 2025, 114-126

P-ISSN: 1858-2281; E-ISSN: 2442-3998

Estimation of 2021 M7.3 Flores Sea Earthquake Displacement Derived from Static GNSS Observation

Putra Maulida*[1], Yola Asis Herawati[1], Putra Rizkiya[2], Sari Rizky[3], Akbar Kurniawan[1], Safanata Azza Laksono[1], Yanto Budisusanto[1],

[1]Department of Geomatics Engineering, Faculty of Civil Planning and Geo-Engineering, ITS, Surabaya, 60111, Indonesia
[2]Architecture and Planning Department, Faculty of Engineering, Universitas Syiah Kuala, Banda Aceh, Indonesia
[3]Department of Chemistry, Faculty of Science and Technology, Universitas Samudra, Langsa 24416, Indonesia

*Corresponding author: putra@its.ac.id

Accepted: DDMMYYYY; Revised: DDMMYYYY; Accepted: DDMMYYYY; Published: DDMMYYYY

Abstract: On 12 December 2021, a Mw 7.3 strike-slip earthquake ruptured a previously unmapped fault in the Flores Sea, later identified as the Kalaotoa fault. The event damaged 345 buildings and displaced nearly 3,900 residents, highlighting the seismic hazard in the Sunda–Banda arc transition zone. In this study, we analyzed static GNSS data from the Indonesian Continuously Operating Reference System (InaCORS) to estimate coseismic displacements. Daily coordinate solutions, corrected for satellite orbit, ionospheric, and tropospheric errors, were processed to extract the coseismic offsets during the event. Results show horizontal displacements of up to 30 mm at CFLT, 22 mm at CMRE, and 19 mm at CUKA, with vertical motions reaching ~13 mm uplift at CUKA and ~9 mm subsidence at CMRE, which suggests that the earthquake not only incorporates the strike-slip movement but also the dipping movement. Stations near the epicenter moved northwestward, while northern stations moved southeastward, consistent with a right-lateral strike-slip mechanism. To validate the observations, we employed a half-space elastic dislocation model based on centroid moment tensor solutions for fault geometry. The model reproduced the general displacement patterns but showed systematic discrepancies, including overestimation of horizontal offsets by nearly a factor of two at near-epicenter stations (CFLT, CMRE, CUKA, CLWB) and underestimation of vertical motions by up to 20–30 mm. The misfit corresponds to an RMSE of ~10 mm for horizontal and ~30 mm for vertical displacement. These results indicate that a single homogeneous slip model oversimplifies the rupture, suggesting the need for more complex fault segmentation or slip inversion. Overall, this study demonstrates the capability of GNSS to capture coseismic deformation robustly and emphasizes its importance for refining earthquake source models and improving seismic hazard assessment in tectonically complex regions such as eastern Indonesia.

keywords: Flores Sea earthquake; GNSS; static displacement; half-space model

How to cite: Maulida, P., Herawati Y A., Rizkiya, P., Rizky S., Kurniawan A., Laksono S A., (2025). Estimation of 2021 M7.3 Flores Sea Earthquake Displacement Derived from Static GNSS Observation. *Geoid, 15(1), 114-126.*

Introduction

Located between the Sunda-Banda arc transition zone, the Flores and Sumba islands are prone to earthquakes. The area is characterized by the unique tectonic regime of the eastern part of the subduction of the Sunda arc and the western part of the Banda arc collision with the Australian plate (Hall, 2002). In this area, due to the compression of the Australian plate, which moves approximately 74 mm/yr with respect to the Sunda plate, a thrust earthquake is commonly found (Ekstrom et al., 2012). The earthquake was attributed to the back-arc fault along Flores and Wetar. The example of a fault system is the Flores back-arc thrust, which extends from the north to the west to the Kendeng-Baribis thrust fault (Koulali et al., 2016). Due to the thin crust along this region, the strike-slip fault is facilitated by the partitioning of the convergence area (McCaffrey, 1998). The existence of a complex tectonic regime has led to numerous damaging earthquakes occurring in this region,

characterized by different focal mechanisms. During the last century, several large earthquakes occurred in this region, producing tsunamis, including the 1977 M8.3 event. The historical event demonstrated that many earthquakes occur in association with the subduction zone and thrust fault system. Indonesia Earthquake Study Center (PuSGeN) mapped several strike-slip earthquakes in the region (Irsyam et al., 2017). Hence, in this region, a strike-slip fault accommodates the north-south convergence, which is also responsible for the inland earthquake in the past, such as the 2015 M6.5 Alor earthquake (Xu et al., 2015). The Alor earthquake is responsible for the 241 damage to housing and buildings in the vicinity. This event indicates the possibilities of the existence of a strike-slip fault that might be yet unmapped in this area, which might change the current seismic hazard analysis.

In 2021, different from the Alor earthquake, a M7.3 earthquake occurred north of the Sunda-Banda arc transition zone on 12 December 2021. The earthquake caused damage to 345 buildings and forced 3900 refugees. The shaking triggered by a strike-slip mechanism earthquake, which is sourced from a previously unmapped fault. Supendi et al. (2022) relocated the earthquake distribution and proposed that the newly identified fault consists of three segments. The previous result already identified the fault source, which is known as the Kalaotoa fault. Even though the fault has been well identified, the effect of the coseismic slip is totally unmapped. Coseismic slip can cause displacement at a point on the Earth's crust. The displacement on the Earth's surface can be estimated using the paleoseismology method by compiling the morphology of the Earth based on the Light Detection and Ranging (LIDAR) data and terrain model (Daryono et al., 2019), especially for historical earthquakes; seismic data (Supendi et al., 2022), and InSAR (Meilano et al., 2021), but the most robust is by utilizing Global Navigation Satellite System (GNSS) observation (Gunawan et al., 2022). GNSS showed promising observation due to high temporal sampling, which can reach sub-second intervals, and is installed for an extended period. The development of GNSS monitoring enables the capture of the entire earthquake cycle, which occurs over both very short and long periods, by estimating the daily position over an extended period. Every motion due to tectonic and non-tectonic motion can be captured (Govers et al., 2018). The current GNSS installation in Indonesia has been used to estimate the interseismic coupling and potential of earthquake magnitude (Hanifa et al., 2014), long-period deformation (Rahmadani et al., 2022), coseismic slip which caused the earthquake, the early afterslip, and long viscoelastic deformation due to the mantle wedge (Gunawan et al., 2014). Hence, the current system of earthquake early warning also utilizes GNSS observations as a complement for reliable early tsunami prediction (Ohta et al., 2012).

In this study, we utilized the continuous GNSS installed by the Indonesian Geospatial Agency (BIG) to investigate the coseismic deformation due to the M7.3 Flores Sea Earthquake. Previous research has shown promising results using GNSS observations to estimate the earthquake source or validate previously developed earthquake models (Maulida et al., 2015; Gunawan et al., 2016). We estimate the coseismic displacement based on GNSS using the daily GNSS data. To validate the displacement, we compare it with the theoretical displacement employed using the half-space model (Okada, 1985). By conducting this study, the development of earthquake monitoring can include GNSS observation to estimate the earthquake source and contribute to mitigating future earthquake disasters, especially for previously unmapped fault systems.

Data and Methodology

Since 2019, BIG has expanded the number of Indonesia Continuously Operating Reference System (CORS) stations along the Indonesian archipelago. This installation has significantly enhanced the ability to record more earthquake events based on geodetic data, particularly the event of 14 December 2021. Due to the installation development, only several InaCORS were available during the M7.3 Flores Sea Earthquake. We analyze the RINEX format data using a daily static processing strategy. Thus, for the static process, we use the processed 42 InaCORS stations time series by Maulida et al. (2024) (Figure 1), which are located along the Flores back-arc thrust using GAMIT-GLOBK 10.7 (Herring et al., 2010). We comprehensively include several correction data to improve the processing quality. We utilize the final precise orbit products derived by IGS to fix the satellite orbit. We also apply the second-order ionospheric correction, and we utilize the Vienna Mapping Function (VMF1) to estimate the tropospheric delay parameters. The brief explanation of processing strategy is showed as figure 2. To obtain a consistent coordinate in ITRF2014, we also processed the IGS stations located surrounding the Indonesian archipelago (Figure 3).

We first fit the time series using equation (i) considering linear trend, periodic motion and sudden offset (Nikolaidis, 2002). We obtain a clean time series and then remove the outlier using 3σ. The cleaned time series is used to extract the coseismic offset. We practically estimate the coseismic displacement using a five-day difference before the M7.3 Flores Sea earthquake occurrence and after the earthquake occurrence. The sign of the earthquake is clearly shown by the sudden offset in the time series of GNSS stations.

$$y(t_i) = a + bt_i + c\ sin(2\pi t_i) + d\ cos(2\pi t_i) + e\ \sin(4\pi t_i) + \mathrm{f}\cos(4\pi t_i) + \sum_{j=1}^{n_g} g_j\, H\left(t_i - T_{gj}\right) \qquad (1)$$

In which, a is the offset of the time-series, b is the linear slope during, which reflect the interseismic velocity, c and d are amplitude of annual periodic signal, while e and f refer to the semiannual signal, g refer to the offset to the antenna change or coseismic offset displacement that can be easily distinguish via https://srgi.big.go.id/visual_gnss.

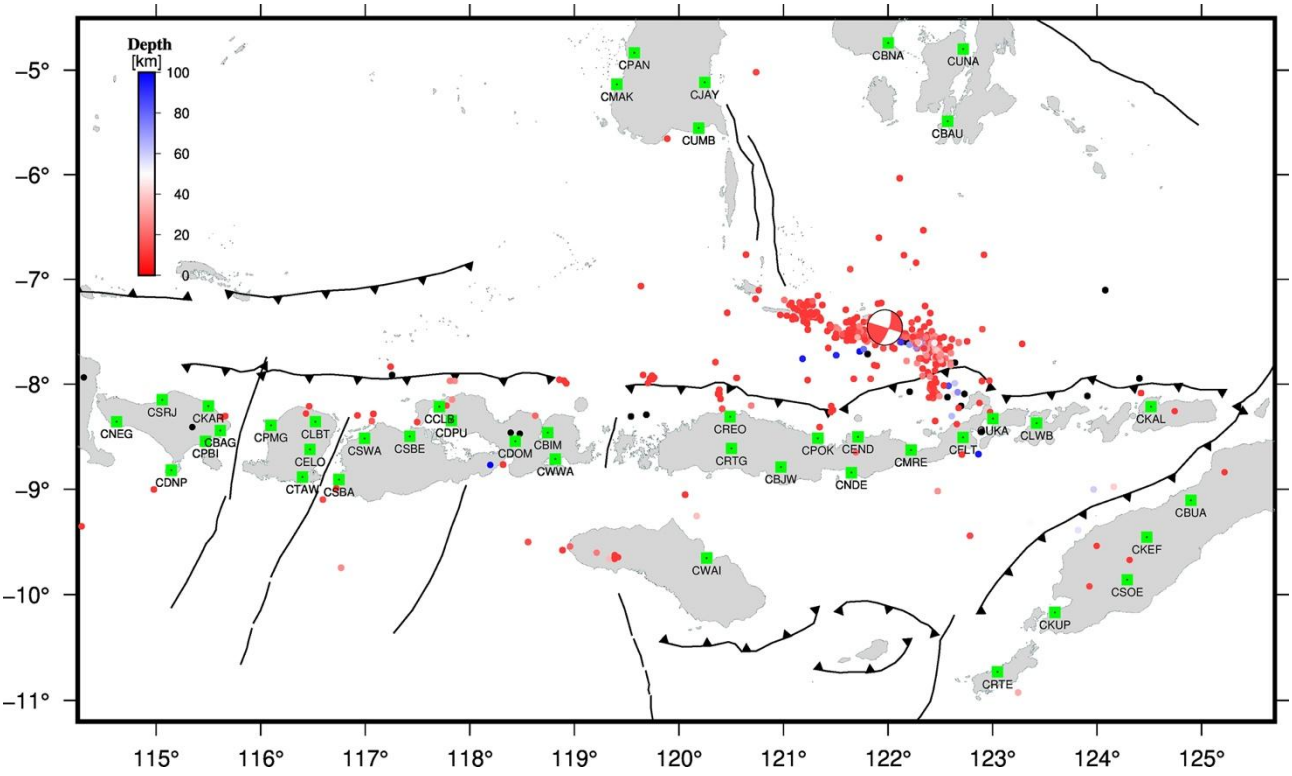

Figure 1. InaCORS distribution used for the processing represented by a green square; the circle denotes the earthquake distribution that occurred from 14 December to 24 December 2021, with the color representing the earthquake depth shown in the colorbar.

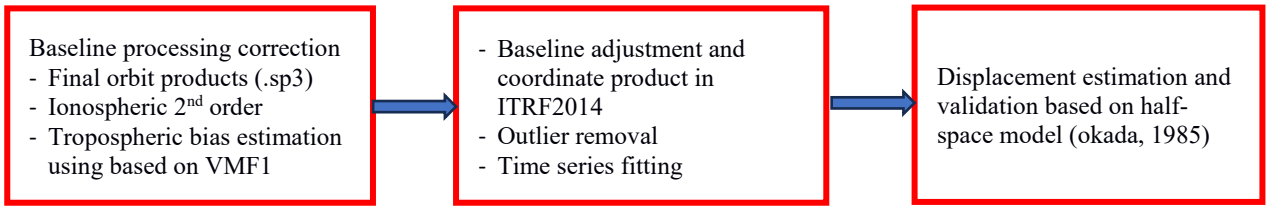

Figure 2. Simple flowchart for GNSS processing using GAMIT and displacement analysis

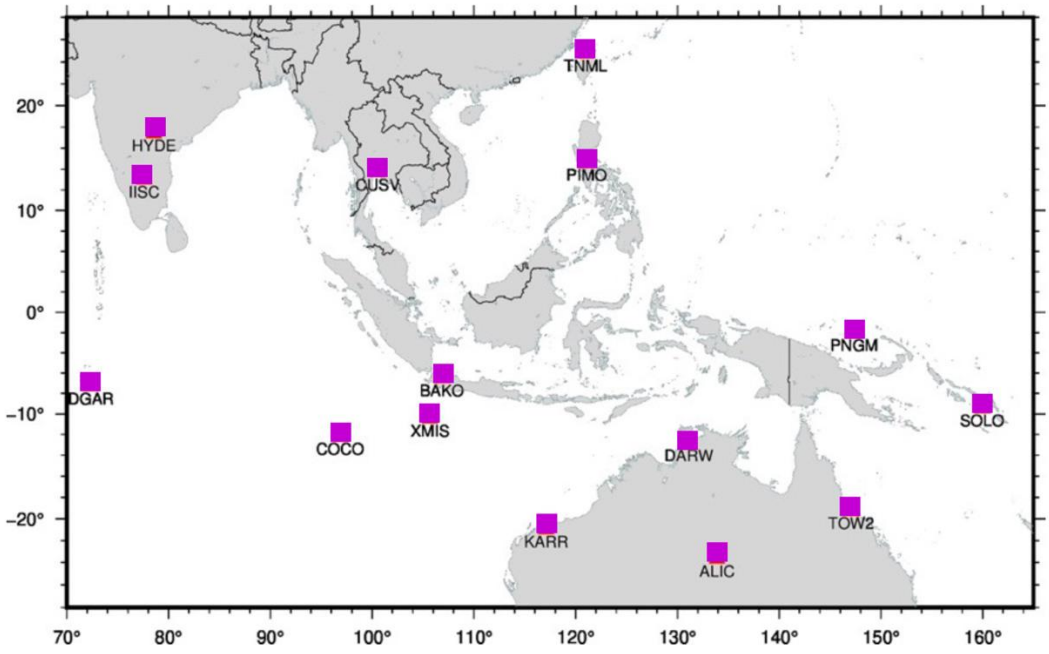

Figure 3. IGS stations Distribution for processing

As additional data, we also used the earthquake distribution with the same duration as the GNSS data of Maulida et al. (2024), which is from 2019 to 2023. However, due to the background noise, we used the earthquakes that occurred during the ten days after the Flores 2021 M7.3 mainshock. The data was obtained from the Indonesian Meteorology, Climatology, and Geophysics Agency (BMKG) catalogue. The earthquake concentration aligns with the main earthquake location and can be easily used to distinguish the newly formed fault. The distribution of the aftershocks reflects the newly formed fault, which is not yet mapped. For the orientation and geometry of the fault moment, we used the centroid-moment-tensor data from Supendi et al. (2022). The previous research estimated the depth dip, strike, and rake angle to be 12.19 km, 288°, 78°, and 169°, respectively. Based on the geometry model, we perform the forward calculation based on the half-space model (Okada et al., 1985). Then we compare the modelled displacement with the GNSS station displacement.

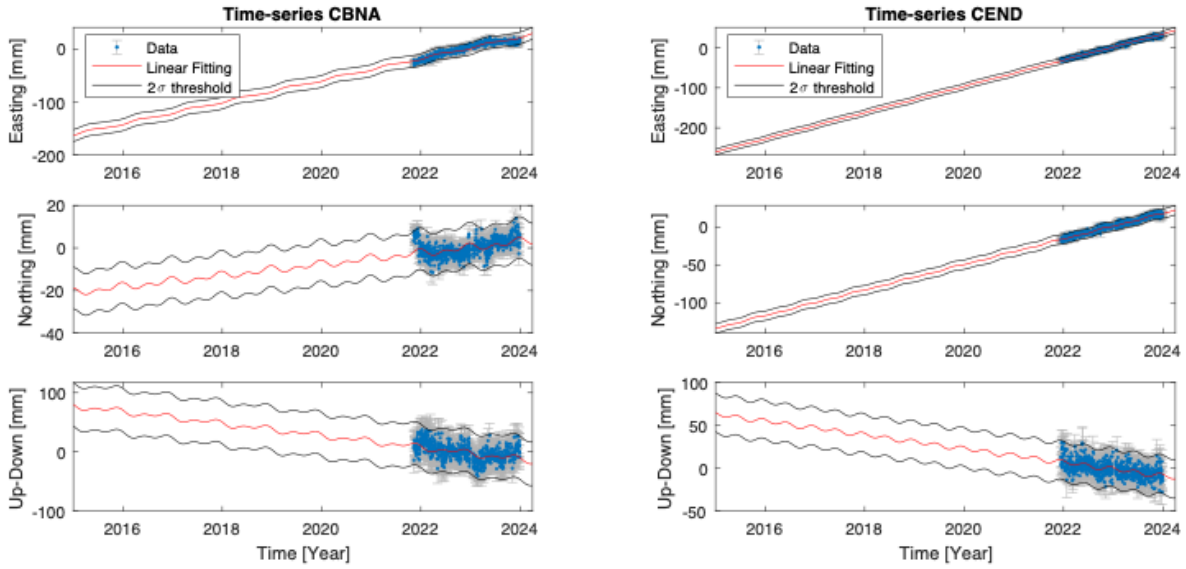

Figure 4. Cleaned time series after removing 3σ outliers

Result and Analysis

a. Coseismic displacement estimation

We estimate the displacement due to the Flores Sea earthquake based on GNSS data. Figure 5 shows the time series for several stations during the 5 days before and after the earthquake. The time series of station coordinates is displayed in topocentric coordinates to represent the actual movement of the physical Earth. The time series clearly captures the coseismic displacement. The earthquake displacement is presented as an offset in the GNSS time series.

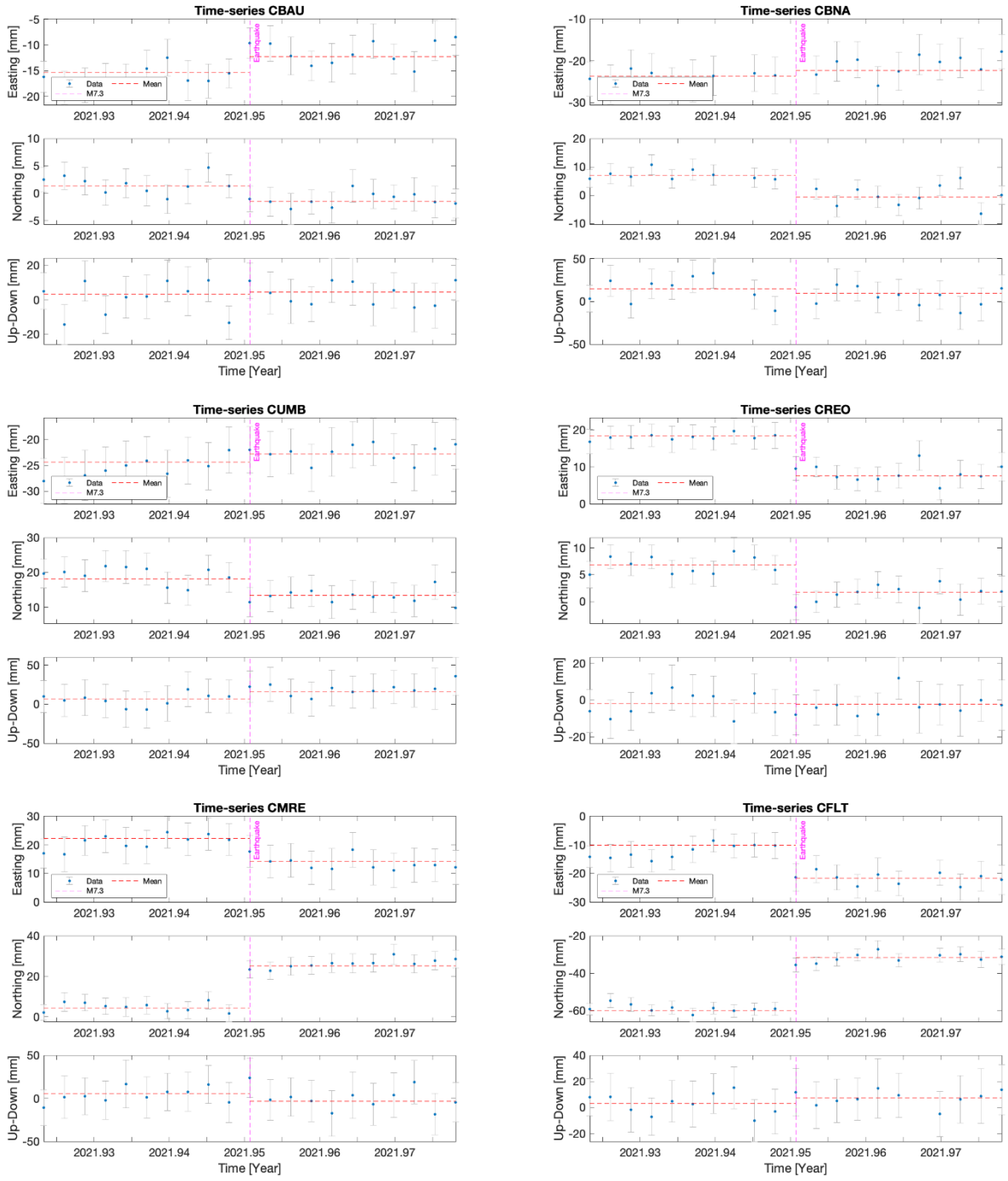

Figure 5. Time series of several GNSS stations: CBAU, CBNA, CUMB, CREO, CMRE, CFLT

The earthquake is a sudden energy release that accumulated during a period and ruptured in less than several minutes; in this earthquake, it lasted for 30 seconds. This offset might show up in a time series based on its

magnitude, usually for a minimum M6 earthquake, but also depends on the station location to the epicenter. In Figure 4, the timing of the earthquake is represented by a purple dashed line. We found the most significant offset at the station, up to 30 mm and 10 mm for horizontal and vertical displacement, respectively. The most significant displacement is found at station CFLT, which reaches 30 mm, CMRE for 22 mm, and CUKA 19 mm, which is located 112 km from the epicenter. The displacement for several other GNSS stations can be found in Table 1. The GNSS stations located close to the epicenter show northwest displacement: CMRE, CUKA, CFLT, and CLWB, which are south of the earthquake source.

Meanwhile, toward the western part of the Flores Island, the rest of the station shows a southwest direction with a displacement of less than 15 mm. We also incorporated the stations in the north, which are located south of Sulawesi Island. The displacement was directed in the southeast direction, with the most significant displacement being up to 10 mm. The pattern of horizontal displacement shows a clear association with the strike-slip mechanism earthquake. Based on earthquake distribution, Supendi et al. (2022) suggest a right-lateral fault that consists of three segments that might have accumulated into a single static displacement.

Table 1. Coseismic displacement due to M7.3 Flores Sea Earthquake

Station	dE (mm)	dN (mm)	dU (mm)	sdE (mm)	sdN (mm)	sdU (mm)
CFLT	-11.5	28.2	4.4	6.4	5.2	24.5
CMRE	-8.1	20.8	-8.9	8.4	6.1	33.6
CUKA	-8.1	17.7	13.1	6.6	5.3	27.0
CPOK	-14.2	-4.7	-8.1	5.2	4.1	19.5
CREO	-10.7	-5.2	-0.2	4.6	3.4	15.8
CEND	-11.0	3.5	-2.8	5.0	3.9	18.9
CLWB	-3.2	10.2	-4.3	5.9	4.5	21.4
CRTG	-8.6	-4.8	5.2	7.1	6.4	30.8
CBJW	-8.8	-1.2	-0.6	4.6	3.7	17.9
CBNA	1.4	-7.7	-5.4	6.9	5.4	26.6
CSOE	-5.1	5.3	-8.1	11.0	8.3	46.0
CPAN	4.3	-3.9	-2.0	7.5	5.7	29.9

The displacement pattern of all GNSS stations can be found in Figures 6 and 7 for horizontal and vertical displacement, respectively. However, although the mechanism of the earthquake is strike-slip, we can still find the vertical motion. The station, which previously had significant horizontal motion, also indicates the vertical movement, although the error is quite large, apparently more than 10 mm. We found uplift at station CFLT, CMRE, CUKA, and CLWB. It appears that the station located southeast of the earthquake epicenter is uplifted; meanwhile, stations north of the epicenter are subsiding. To the west of the epicenter, the displacement is subsidence as shown from station CPOK. In addition, the station located in the west, about 300 km from the epicenter, has a relatively small vertical motion, less than 1 mm. Based on the mechanism, the earthquake geometry for dip angle is 78°, which might produce the vertical movement pattern due to the existence of slope on fault interface. This vertical displacement will be impossible to appear on the strike-slip-only fault in which the dip is almost 90°. It is also consistent with the generation of a sudden 90 mm increase at sea level (Sudjono et al., 2024). In addition, during this processing, the data used is the daily coordinate solution, so the coseismic derived from this time series is the cumulative coseismic of all earthquakes that occurred on the same observation day. The vector of displacements is the summation of the earthquake sequence. The displacement might also be contaminated with the early postseismic deformation. Some large earthquakes trigger afterslip that accounts for ~10% of the coseismic displacement within the first 12 hours (Twardzik et al., 2019). Therefore, postseismic effects are still recorded in the daily coseismic shifts. Additionally, it is worth noting that the coseismicity from the daily data also accounts for the influence of local surface displacements. Some earthquakes that occur on land also trigger local displacements, such as the M7.5 Palu-Donggala earthquake in 2018 (Jalil et al., 2021).

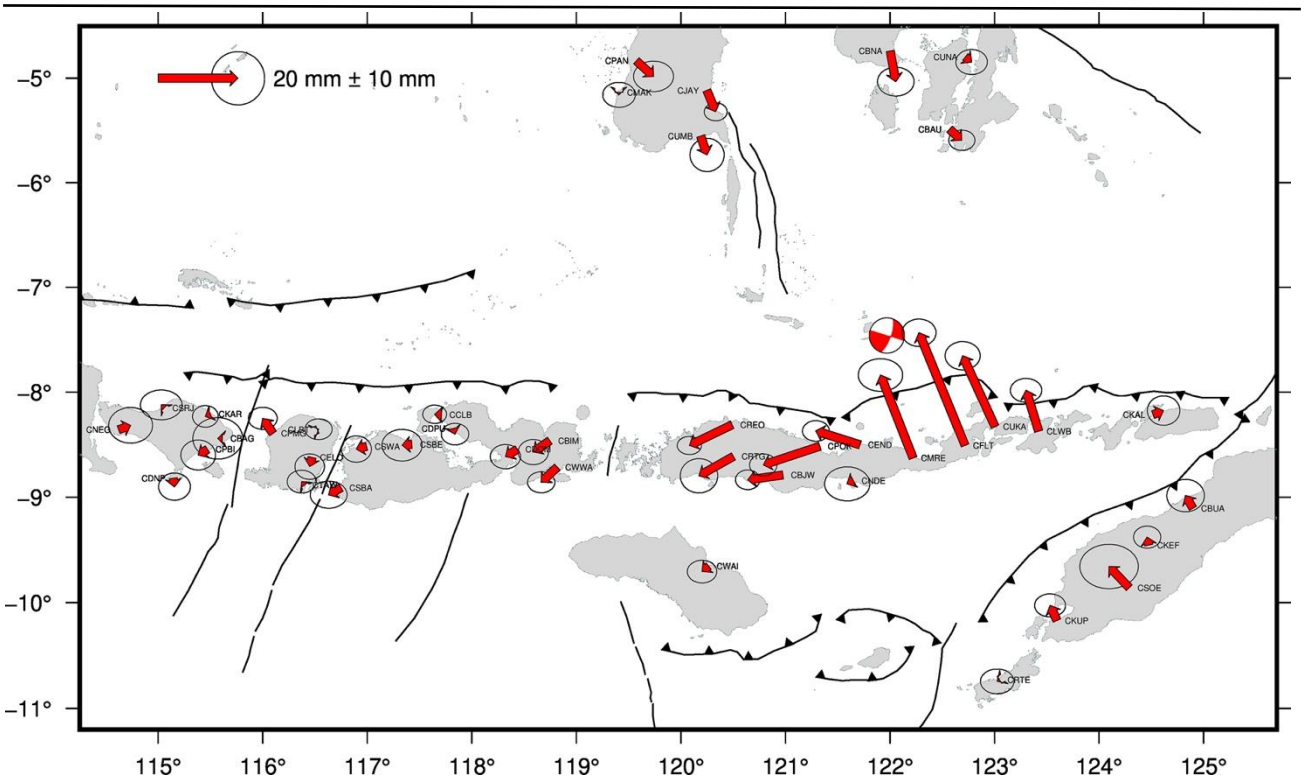

Figure 6. Horizontal coseismic displacement of M7.3 Flores Sea Earthquake

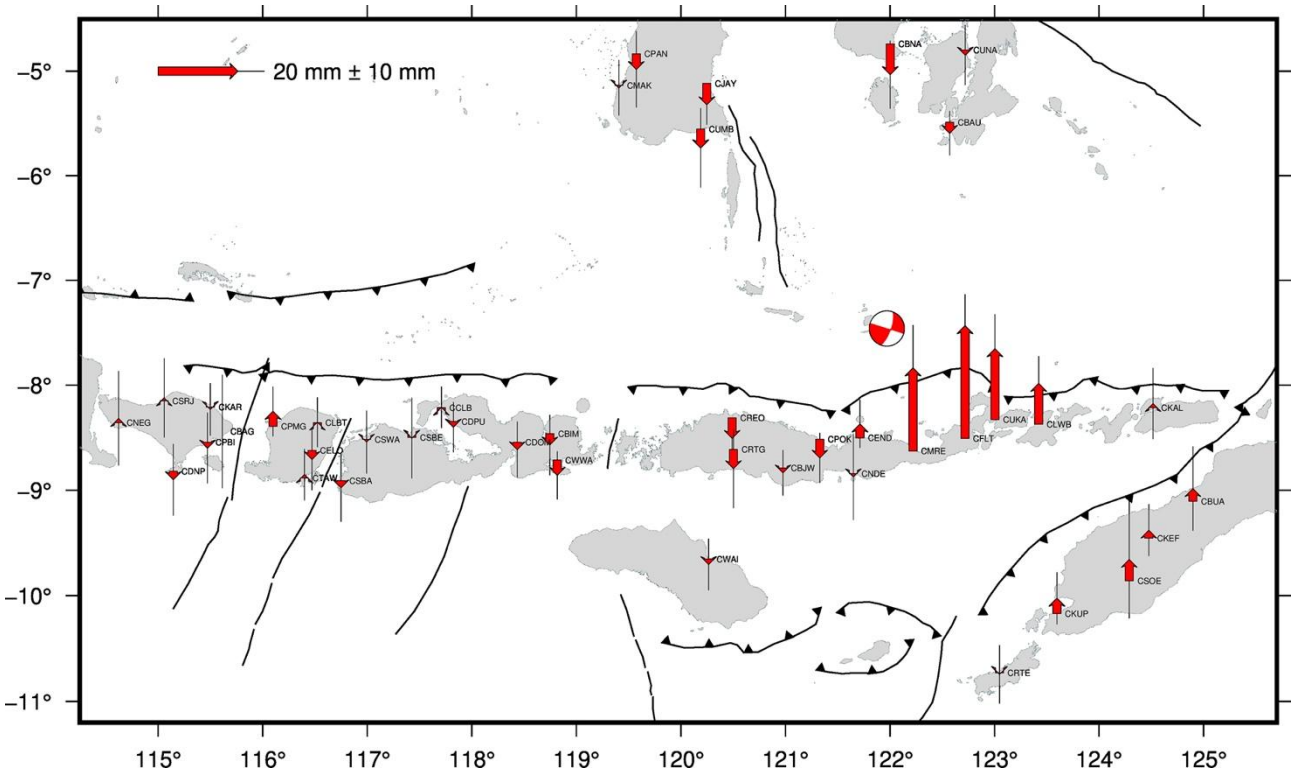

Figure 7 Vertical coseismic displacement of M7.3 Flores Sea Earthquake

To validate the earthquake displacement, we perform a forward calculation based on the half-space model (Okada, 1985). We firstly construct the earthquake geometry based on Supendi et al. (2022) and calculate the empirical length, width of the fault, and the slip of the earthquake. We calculate using equation (2~5). The

equation is an empirical formula used to calculate the seismic field from earthquake magnitude, based on the work of Well and Coppersmith (1994), Kanamori and Rivera (2004), and Papazachos et al. (2004). M_w is the earthquake magnitude, Mo is the moment magnitude in Nm, D is the surface area of the seismic field in km^2, S is the slip in meters, and L is the length of the seismic field in the strike direction. In the simulation, we consider the convention of strike as fault trace direction (0 to 360° relative to North), defined so that the fault dips to the right side of the trace and the rake as the direction the hanging wall moves during rupture, measured relative to the fault strike.

$$Mw = \frac{2}{3} logMo - 6.07 \tag{2}$$

$$Mw = 4.07 + 0.98 \log D \tag{3}$$

$$Mo = \boldsymbol{\mu} DS \tag{4}$$

$$\log(L) = 0.58Mw - 2.3 \tag{5}$$

Based on equations (2~5), we set the geometry of the earthquake as shown in Table 2:

Table 2. Parameter given for model calculation based on the half-space model (Okada, 1985)

Parameters	Value	Source
Length	85.90 km	Calculated
Width	23.01 km	Calculated
Depth	12.19 km	Supendi et al. (2022)
Strike	288°	Supendi et al. (2022)
Dip	78°	Supendi et al. (2022)
Rake	169°	Supendi et al. (2022)
Slip	1.914 m	Calculated

The simulated displacement of the M7.3 Flores Sea Earthquake can be found in Figures 7 and 8 for horizontal and vertical displacement, respectively. The horizontal displacement shows a consistent pattern between the data and the model. However, we find significant discrepancies on the stations that are located south of the fault, specifically on station CMRE, CUKA, CFLT, and CLWB, with rms up to 10 mm. Meanwhile, for the station located at the west and north side, the displacement shows the southwest and southeast motion, respectively, which also agrees with the data. Based on the simulation, the stations located southeast of the epicenter indicate northwest motion of almost 50 mm, two times larger than the data. However, we can fit the station located on the west and north sides of the epicenter, which is less overestimated compared to the station located very close to the epicenter (CFLT, CMRE, CUKA, and CLWB). The simulation also noted an important line that the earthquake caused vertical motion, which is consistent with the data (Figure 8). In contrast to the horizontal motion, the vertical motion is likely underestimated for the model for the near epicenter station. At station CEND, the motion indicates a contrast between data and model, because the station is in the middle of the gradual pattern of uplift to subsidence on Flores Island. Compared to the data, the model indicates no motion less than 1 mm in the Nusa Tenggara Barat region. It strongly shows that no motion appears at far-off stations.

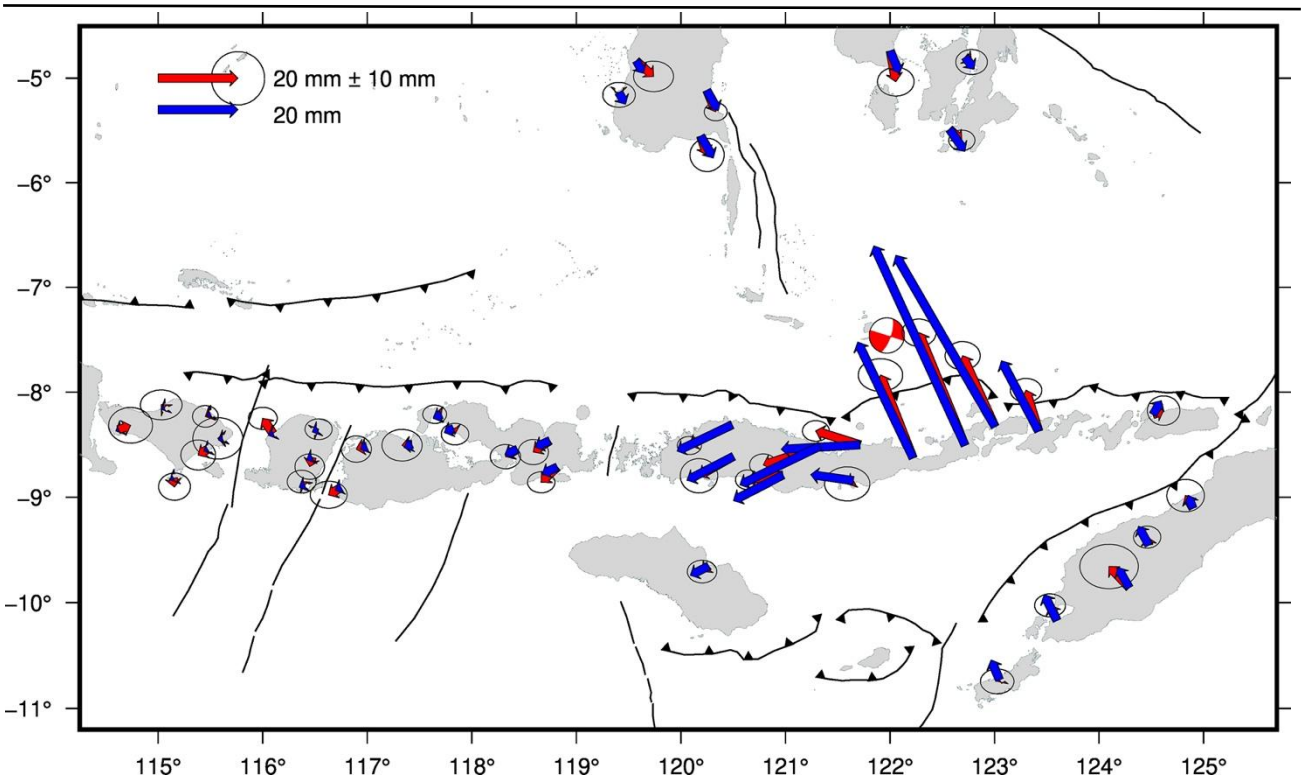

Figure 8. Horizontal coseismic displacement of M7.3 Flores Sea Earthquake, in which the red arrow represents observation, while the blue arrow represents the model

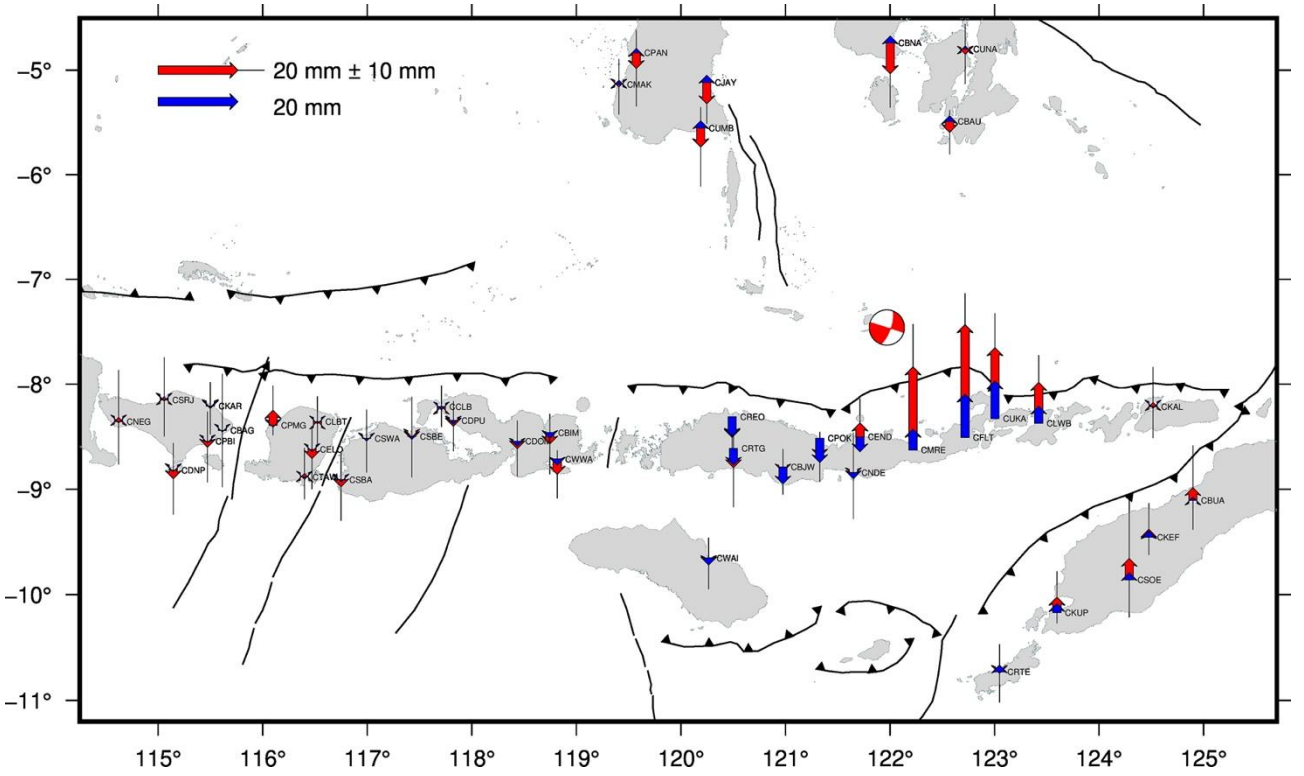

Figure 9. Vertical coseismic displacement of M7.3 Flores Sea Earthquake, in which the red arrow represents observation, while the blue arrow represents the model

The residual between the data and the model for the station with significant motion is shown in Table 3. The discrepancies might indicate that the over- and underestimation of the forward modelling is related to the given parameters. This might refer to the centroid coordinate of the rectangular fault, which, in this simulation, is aligned with the earthquake epicenter and the geometrical parameters. Firstly, we fixed the length and width of the fault model to a single, significant finite fault measuring 88 km in length and 24 km in width. Secondly, the slip model is also based on empirical considerations, with a magnitude of 7.3 produced by a 1.9 m slip at the source. Although the geometrical model of fault orientation is more reliable, the assumption of fault length may lead to over- or underestimation of the results. The result is also affected by a single slip-homogeneous fault; meanwhile, in other cases, a more complex fault model, especially for a strike-slip event, is a better fit than a simple one (Hill et al., 2015; Gunawan et al., 2016). For the next work, the inversion method for better estimation of the slip model will be critical to assess the hazard to the Nusa Tenggara Timur and Nusa Tenggara Barat region, because likely in the area, the earthquake assessment only considers the Flores Back-Arc Thrust.

Table 3. Residue between data and model

Station	Residue horizontal displacement (m)	Residue vertical displacement (m)
CFLT	-0.0115	0.0282
CMRE	-0.0081	0.0208
CUKA	-0.0081	0.0177
CPOK	-0.0142	-0.0047
CREO	-0.0107	-0.0052
CEND	-0.0110	0.0035
CLWB	-0.0032	0.0102
CRTG	-0.0086	-0.0048
CBJW	-0.0088	-0.0012
CBNA	0.0014	-0.0077
CSOE	-0.0051	0.0053
CPAN	0.0043	-0.0039

Several studies have analyzed coseismic displacement and the influence of postseismic earthquakes that occur within a few hours after an earthquake (Twardzik et al., 2019). The analysis of GNSS observation data was conducted using epoch-by-epoch kinematic data compared to daily data. By using epoch-by-epoch data, details of earthquake motion at GNSS stations within minutes or even seconds can be analyzed, both coseismic and postseismic motion. One of the drawbacks of kinematic analysis is that sources of error that could have been averaged out in daily processing will appear with larger amplitudes. A suitable processing strategy is necessary to mitigate the effects of the troposphere and multipath that can contaminate kinematic GNSS data. Although kinematic data can describe the post-earthquake phases in detail, seismicity analysis with geodetic data relies heavily on a dense distribution of GNSS observation networks. In this study, the scarcity of GNSS stations near the Pasaman earthquake source is one of the obstacles to further analyzing the characteristics of earthquakes on the Sumatra fault. One way to overcome this is to use a combination of GNSS data and InSAR (interferometric Synthetic Aperture Radar) observation data. InSAR data can support GNSS observation data to constrain earthquake geometry and calculate slip at the earthquake source in more detail (Ghayournajarkar & Fukushima, 2020).

b. Effect on the current Seismic Hazard Analysis

The 2021 Mw 7.3 Flores Sea earthquake highlights the importance of integrating geodetic evidence into regional seismic hazard assessments, particularly for coastal cities in eastern Indonesia. The GNSS-derived displacement results, showing horizontal shifts up to 30 mm and vertical motions exceeding 10 mm near the epicenter, demonstrate that even moderate-to-large magnitude strike-slip events can generate measurable crustal deformation with potential cascading impacts on the built environment (Avallone et al., 2011). Such deformation poses risks not only to housing and public infrastructure but also to critical lifelines such as ports, roads, and energy networks that support the regional economy.

Earthquakes pose a risk to the city planning and environmental section. From a city planning perspective, the findings emphasize the need for stricter enforcement of earthquake-resistant building codes and zoning

regulations in areas near active fault systems (Izadkhah et al., 2010). Urban expansion in coastal zones, particularly in Flores, Alor, and surrounding islands, should account for the potential of both ground shaking and secondary hazards such as liquefaction, subsidence, and coastal instability, considering the liquefaction at the previous Palu Earthquake 2018 (Tanjung et al., 2023). Incorporating GNSS monitoring into early warning and hazard mapping systems would enable local governments to identify high-risk areas better and prioritize the development of resilient infrastructure (Ruhl et al., 2027). Environmental considerations are also crucial, as coseismic displacement in coastal settings may alter groundwater dynamics, accelerate coastal erosion, and modify ecosystems that communities depend on for fisheries and agriculture. Disruption of mangrove belts, coral reefs, and low-lying wetlands could amplify vulnerability to tsunamis and storm surges (Mavroulis et al., 2023). Therefore, hazard-informed land-use planning must be combined with ecosystem-based adaptation strategies, such as preserving natural coastal buffers, to strengthen disaster resilience.

Overall, the coseismic deformation derived in this study provides not only scientific insight into fault behavior but also practical guidance for reducing disaster risk. By integrating geodetic data into seismic hazard assessment, city planning, and environmental management, local authorities can improve preparedness and ensure sustainable development in tectonically active regions of eastern Indonesia.

Conclusions

We have investigated the coseismic displacement due to the M7.3 Flores earthquake based on GNSS observations, that is not previously done:

- The GNSS observations show a pattern of consistent strike-slip motion with a vertical motion due to the fault geometry. The displacement of GNSS at stations located close to the epicenter is northwest with horizontal up to 30 mm and uplift up to 10 mm. Meanwhile, stations located north of the epicenter indicate southeastward motion. The displacement is also sighted at the GNSS located north of Sulawesi Island, indicating a broad deformation affected around the fault center. The GNSS station located off to the west, close to Bali Island, is not affected by the earthquake motion.
- In addition, we also performed the forward calculation based on a single homogeneous fault model. Our result shows that the data can fit the pattern of displacement for both vertical and horizontal motion. The model and data show that the displacement is consistent with strike-slip motion. The overall RMSE for horizontal is 10 mm, while vertical motion is 30 mm. These results emphasize the usage of a single fault model for early analysis but somehow did not satisfy the whole observation due to the complexity of the fault motion.
- We emphasize the usage of GNSS observations as part of earthquake monitoring to reduce the number of damage and loss. GNSS enables the capture of the motion of moderate earthquakes, which possibly produce more hazards to the city.

Acknowledgements

The authors would like to thank the Indonesia Geospatial Agency (BIG) for providing easy access to INACORS. Some of the images in this study used GMT (Generic Mapping Tools) software.

References

Avallone, A., Marzario, M., Cirella, A., Piatanesi, A., Rovelli, A., Di Alessandro, C., ... & Mattone, M. (2011). Very high rate (10 Hz) GPS seismology for moderate-magnitude earthquakes: The case of the Mw 6.3 L'Aquila (central Italy) event. Journal of Geophysical Research: Solid Earth, 116(B2).

Daryono, M. R., Natawidjaja, D. H., Sapiie, B., & Cummins, P. (2019). Earthquake geology of the lembang fault, West Java, Indonesia. Tectonophysics, 751, 180-191.

Ekström, G., Nettles, M., & Dziewoński, A. M. (2012). The global CMT project 2004–2010: Centroid-moment tensors for 13,017 earthquakes. Physics of the Earth and Planetary Interiors, 200, 1-9.

Ghayournajarkar, N., & Fukushima, Y. (2020). Determination of the dipping direction of a blind reverse fault from InSAR: case study on the 2017 Sefid Sang earthquake, northeastern Iran. Earth, Planets and Space, Vol: 72, Hal: 1-15.

Govers, R., Furlong, K. P., Van de Wiel, L., Herman, M. W., & Broerse, T. (2018). The geodetic signature of the earthquake cycle at subduction zones: Model constraints on the deep processes. Reviews of Geophysics, 56(1), 6-49.

Gunawan, E., Kholil, M., & Widiyantoro, S. (2022). Coseismic slip distribution of the 14 January 2021 Mamuju-Majene, Sulawesi, earthquake derived from GPS data. Natural Hazards, 111(1), 939-948.

Gunawan, E., Maulida, P., Meilano, I., Irsyam, M., & Efendi, J. (2016). Analysis of coseismic fault slip models of the 2012 Indian Ocean earthquake: Importance of GPS data for crustal deformation studies. Acta Geophysica, 64(6), 2136-2150.

Gunawan, E., Sagiya, T., Ito, T., Kimata, F., Tabei, T., Ohta, Y., ... & Sugiyanto, D. (2014). A comprehensive model of postseismic deformation of the 2004 Sumatra–Andaman earthquake deduced from GPS observations in northern Sumatra. Journal of Asian Earth Sciences, 88, 218-229.

Hall, R. (2002). Cenozoic geological and plate tectonic evolution of SE Asia and the SW Pacific: computer-based reconstructions, model and animations. Journal of Asian earth sciences, 20(4), 353-431.

Hanifa, N. R., Sagiya, T., Kimata, F., Efendi, J., Abidin, H. Z., & Meilano, I. (2014). Interplate coupling model off the southwestern coast of Java, Indonesia, based on continuous GPS data in 2008–2010. Earth and Planetary Science Letters, 401, 159-171.

Herring, T. A., King, R. W., & McClusky, S. C. (2010). Introduction to gamit/globk. Massachusetts Institute of Technology, Cambridge, Massachusetts, 400, 401.

Hill, E. M., Yue, H., Barbot, S., Lay, T., Tapponnier, P., Hermawan, I., ... & Sieh, K. (2015). The 2012 Mw 8.6 Wharton Basin sequence: A cascade of great earthquakes generated by near-orthogonal, young, oceanic mantle faults. Journal of Geophysical Research: Solid Earth, 120(5), 3723-3747.

Izadkhah, Y. O., & Hosseini, M. (2010). Sustainable neighbourhood earthquake emergency planning in megacities. Disaster Prevention and Management: An International Journal, 19(3), 345-357.

Jalil, A., Fathani, T. F., Satyarno, I., & Wilopo, W. (2021). Liquefaction in Palu: the cause of massive mudflows. Geoenvironmental Disasters, 8(1), 21.

Kanamori, H., & Rivera, L. (2004). Static and dynamic scaling relations for earthquakes and their implications for rupture speed and stress drop. Bulletin of the Seismological Society of America, Vol: 94, Hal: 314-319.

Koulali, A., Mcclusky, S., Susilo, S., Leonard, Y., Cummins, P., Tregoning, P., ... & Wijanarto, A. B. (2017). The kinematics of crustal deformation in Java from GPS observations: Implications for fault slip partitioning. Earth and Planetary Science Letters, 458, 69-79.

Maulida, P., Laksono, S. A., Herawati, Y. A., Rizkiya, P., & Kurniawan, A. (2024, December). Analysis of Deformation Along the Flores Back-Arc Thrust Using GPS Observation Data. In IOP Conference Series: Earth and Environmental Science (Vol. 1418, No. 1, p. 012033). IOP Publishing.

Maulida, P., Meilano, I., Gunawan, E., & Efendi, J. (2016, May). Analysis of 2012 M8. 6 Indian Ocean earthquake coseismic slip model based on GPS data. In AIP Conference Proceedings (Vol. 1730, No. 1, p. 040006). AIP Publishing LLC.

Mavroulis, S., Mavrouli, M., Lekkas, E., & Tsakris, A. (2023). Managing earthquake debris: Environmental issues, health impacts, and risk reduction measures. Environments, 10(11), 192.

McCaffrey, R. (1988). Active tectonics of the eastern Sunda and Banda arcs. Journal of Geophysical Research: Solid Earth, 93(B12), 15163-15182.

Meilano, I., Salman, R., Rahmadani, S., Shi, Q., Susilo, S., Lindsey, E., ... & Daryono, D. (2021). Source characteristics of the 2019 M w 6.5 Ambon, eastern Indonesia, earthquake inferred from seismic and geodetic data. Seismological Society of America, 92(6), 3339-3348.

Nikolaidis, R. (2002). Observation of geodetic and seismic deformation with the Global Positioning System. University of California, San Diego.

Ohta, Y., Kobayashi, T., Tsushima, H., Miura, S., Hino, R., Takasu, T., ... & Umino, N. (2012). Quasi real-time fault model estimation for near-field tsunami forecasting based on RTK-GPS analysis: Application to the 2011 Tohoku-Oki earthquake (Mw 9.0). Journal of Geophysical Research: Solid Earth, 117(B2).

Okada, Y. (1985). Surface deformation due to shear and tensile faults in a half-space. Bull. Seismol. Soc. Am, 75(4), 1135-1154.

Papazachos, C. B., Karakaisis, G. F., Scordilis, E. M., & Papazachos, B. C. (2004). Probabilities of activation of seismic faults in critical regions of the Aegean area. Geophysical Journal International, Vol: 159, Hal: 679-687.

Pusat Studi Gempa Nasional (Indonesia). (2017). Peta sumber dan bahaya gempa Indonesia tahun 2017. Pusat Penelitian dan Pengembangan Perumahan dan Permukiman, Badan Penelitian dan Pengembangan, Kementerian Pekerjaan Umum.

Rahmadani, S., Meilano, I., Susilo, S., Sarsito, D. A., Abidin, H. Z., & Supendi, P. (2022). Geodetic observation of strain accumulation in the Banda Arc region. Geomatics, Natural Hazards and Risk, 13(1), 2579-2596.

Ruhl, C. J., Melgar, D., Grapenthin, R., & Allen, R. M. (2017). The value of real-time GNSS to earthquake early warning. Geophysical Research Letters, 44(16), 8311-8319.

Sudjono, E. H., Novico, F., Karima, S., Handiani, D. N., Suhermat, M., Rusdiansyah, A., ... & Setyonegoro, W. (2024, June). Tsunami model of the 2021 Flores earthquake and its impact on Labuan Bajo, East Nusa Tenggara. In *IOP Conference Series: Earth and Environmental Science* (Vol. 1350, No. 1, p. 012032). IOP Publishing.

Supendi, P., Rawlinson, N., Prayitno, B. S., Widiyantoro, S., Simanjuntak, A., Palgunadi, K. H., ... & Arimuko, A. (2022). The Kalaotoa Fault: A newly identified fault that generated the M w 7.3 Flores Sea earthquake. The Seismic Record, 2(3), 176-185.

Tanjung, M. I., Irsyam, M., Sahadewa, A., Iai, S., Tobita, T., & Nawir, H. (2023). Overview of Flowslide in Petobo during liquefaction of the 2018 Palu Earthquake. Soil Dynamics and Earthquake Engineering, 173, 108110.

Twardzik, C., Vergnolle, M., Sladen, A., & Avallone, A. (2019). Unravelling the contribution of early postseismic deformation using sub-daily GNSS positioning. Scientific reports, 9(1), 1775.

Wells, D. L., & Coppersmith, K. J. (1994). New empirical relationships among magnitude, rupture length, rupture width, rupture area, and surface displacement. Bulletin of the seismological Society of America, Vol: 84, Hal: 974-1002.

Xu, G., Wen, Y., Yi, Y., Guo, Z., Wang, L., & Xu, C. (2023). Geodetic constraints of the 2015 M w6. 5 Alor, East Indonesia earthquake: a strike-slip faulting in the convergent boundary. Geophysical Journal International, 235(1), 247-259.